Sensors and Actuators A 287 (2019) 76–83

Contents lists available at ScienceDirect

Sensors and Actuators A: Physical

journal homepage: www.elsevier.com/locate/sna

Spectral analysis for photoacoustic pressure sensor designs: Theoretical model improvement and experimental validation

Timucin Emre Tabaru[a,*], Sekip Esat Hayber[b], Serkan Keser[b], Omer Galip Saracoglu[a,c]

[a] Clinical Engineering Research and Application Center, Erciyes University, Kayseri 38039, Turkey
[b] Department of Electronic and Automation, Ahi Evran University, Kirsehir 40300, Turkey
[c] Department of Electrical and Electronic Engineering, Erciyes University, Kayseri 38039, Turkey

ARTICLE INFO

Article history:
Received 9 October 2018
Received in revised form
13 December 2018
Accepted 31 December 2018
Available online 7 January 2019

Keywords:
Pulsed laser photoacoustic method
Acoustic pressure sensor
Spectroscopy
Frequency domain solution
Photoacoustic wave equation
Theoretical model approach

ABSTRACT

In the pulsed laser photoacoustic (PA) detection and spectroscopy applications, the fundamental frequency of the PA signal produced, and the sensor resonance frequency should be as close as possible to each other so that analyzes from the obtained signals can be performed effectively. In order to determine the fundamental frequency of the PA wave, a theoretical model approach based on the development of the frequency domain solution of the PA wave equation is presented for use in the PA pressure sensor designs. For the validation of the theoretical model approach, a PA experimental setup was established, and measurements were made in distilled water. The theoretical and the experimental PA frequency spectra were determined to be very compatible with each other. Thus, the theoretical model approach was experimentally validated. According to the theoretical model approach, fundamental frequency values obtained from the experimental measurement results were determined with an average accuracy of ∓4.212%. Furthermore, it has been determined that this value has fallen to ∓0.267% in the measurements. With the obtained results from the theoretical model approach, we propose that the PA pressure sensors with the more selective and narrower band can be designed for the more sensitive detection. Moreover, in this study the effects of different laser parameters such that pulse duration, and laser beam width, on the spectral content of the obtained PA signal are analyzed. These analyses will shed light on the vision of acoustic pressure sensor design by helping to select the most optimum parameters for the PA detection.
© 2019 Elsevier B.V. All rights reserved.

1. Introduction

The pulsed laser PA method has become itself a frequently used technique in many areas through its simplicity, high sensitivity, and easy-to-use features. The technique is utilized in a wide range of research fields, such as underwater acoustic sensing [1] to biomedical imaging [2], from trace detection in different materials with photoacoustic spectroscopy (PAS) [3] to non-destructive inspection [4]. In this study, we focused on the applications of the pulsed laser PA method, such as analyte detection, PAS, and material characterization due to its high detection sensitivity. The main mechanism of the PA effect is stretching and relaxation movements caused by optical absorption following the stimulation of the sample with low power laser pulses. As a result of these movements, an acoustic wave is formed propagating in the sample. The method depends on the physical parameters of the material such as optical absorption, thermal expansion, specific heat, and acoustic speed. If any of these parameters change, the response of the acoustic pressure wave will also change. An acoustic sensor design can be performed when the change in the response is detected and associated with the parameter causing the change.

The first research, the formation of sound by the absorption of the laser energy in a liquid has been presented by Askar'yan [5]. Up to this time, many studies of the PA effect have been applied in many areas experimentally and theoretically. Jackson et al. [6] reported a spectroscopic theory based on the photothermal deflection of the laser beam, which can be applied to sensing in solid materials, liquids, gases, and thin films. Rosencwaig [7] reported his works on photoacoustic spectroscopy of solids and biological materials its theory. Oda et al. [8], using the pulsed laser PA method, they detected cadmium with a precision of 14 ppt. Tam presented other interesting applications of photoacoustic detection in his work [9]. El-Akkad et al. [10] determined the optical absorption coefficient of $Hg_{1-x}Zn_xTe$ alloys in the basic absorption region using the PAS. MacKenzie and co-workers [11–14] performed many experiments to detect glucose non-invasively. Camilotti et al. [15] in order to provide specific information about

* Corresponding author at: Clinical Engineering Research and Application Center, Erciyes University, Kayseri, 38039, Turkey.
E-mail address: etabaru@erciyes.edu.tr (T.E. Tabaru).

https://doi.org/10.1016/j.sna.2018.12.050
0924-4247/© 2019 Elsevier B.V. All rights reserved.

the chemical traces of paracetamol in the near-infrared region, a phase-resolved photoacoustic method was applied. The obtained information was presented as a new finding in chemical studies of paracetamol. In the 2000s, this method was also used many times in gas analysis applications [16–18]. Zeninari et al. [19] have detected methane in air pressure or reduced pressure with the PA system developed by using a near-infrared diode laser at 1.65 μm wavelength. In another study, Choi et al. [20] developed a Doppler velocity meter using a CO_2 laser photoacoustic system. With this system, they detect a Doppler frequency shift that can be as little as 50 kHz and a linear relationship between the speed and the shift. Kosterev et al. [21] for NH_3 monitoring, they have designed a gas sensor with a fiber-coupled distributed feedback diode laser based on quartz-enhancement photoacoustic detection. Rück et al. [22] have characterized a photoacoustic NO_2 trace gas detection system which is based on the use of low-cost components. An optimized cell design with 3D printing was utilized in the system. Elia et al. [23] have developed a photoacoustic gas trace sensor for nitric oxide measurement with a detection limit of 500 ppb. Kumar et al. [24] have developed an ultrasonic detection system based on laser photoacoustic spectroscopic technique. In the detection system, they were used for the first time with a specially designed one side open photo-acoustic cell. In another application, Chen et al. have developed a fiber amplifier-resonance the PAS sensor for the detection of acetylene at the sub-ppb level. They have optimized the PAS sensor for resonance frequency for detection of acetylene at a wavelength of 1532.83 nm [25]. Another application area where the PA method is used is imaging applications [26–29]. In understanding the above-mentioned applications and all other PAS investigations, the frequency domain solution of the PA wave equation has an undeniable importance. Nowadays frequency analysis is becoming important in the acoustic sensor design, which is sensitive to the frequency of the acoustic wave generated in the laser-stimulated medium. The frequency domain analysis is performed by means of the frequency solution of the PA wave equation. There are different approaches in the literature for solving this wave equation [30–35]. In addition to the approximate solutions, Erkol et al. [36,37] analytically obtained Gaussian rectangular and radial form solutions without using any approach.

In the PA sensing and spectroscopy applications, the fundamental frequency and the sensor resonance frequency of the PA signal generated for the detection must be as close to each other as possible. Therefore, the fundamental frequency detection is very important. Through the theoretic model approach that we propose, it is possible to design the more narrowband sensors. In this study, a theoretical model approach is presented by improving the frequency domain solution of the PA wave equation previously presented by Erkol et al [36,37]. Thanks to this, results of time and frequency solutions of the PA wave equation are obtained. Then, a PA detection experimental setup was established, and experimental results were obtained with the same parameter values used in the theoretical calculations. Experimentally obtained and theoretically calculated the PA frequency spectra were determined to be very compatible with each other. By this means, our theoretical model approach has been validated. In addition, different laser parameters such as the pulse duration and the beam width were analyzed and the effects of these parameters on the spectral content of the PA wave propagated in the medium were investigated. It is considered that the investigations will help to select the most suitable parameter for the PA pressure sensor designs.

2. Theory of PA pressure sensing

The main mechanism of the pulsed laser PA method is to apply low energy level laser pulses to an absorbing medium. All or a part

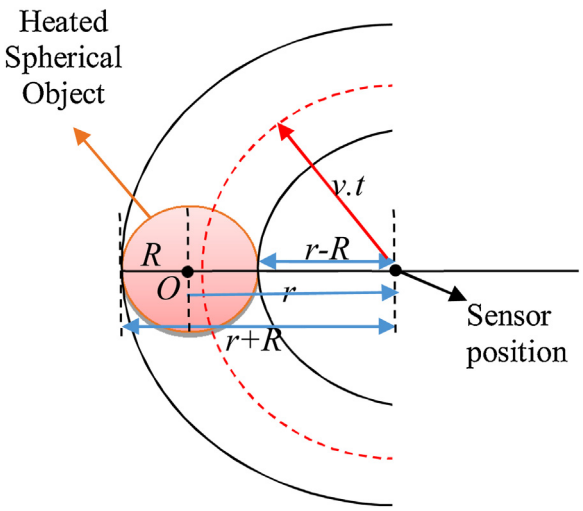

Fig. 1. The SO heated by a laser that is thought to exist in the solutions of PA wave equations in the literature [39].

of the laser pulse energy absorbed by a member of the sample is dispersed in heat form as non-radial relaxation. These periodic heat fluctuations in the sample form an acoustic pressure wave and are detected using suitable pressure detectors. The shape and properties of the PA wave are specified by physical parameters such as the absorption constant of the medium, the thermal expansion constant, the specific heat and the sound velocity of the material. The energy density absorbed in the sample is proportional to the amplitude of the acoustic wave while laser parameters and boundary conditions determine the shape of the wave [38]. The general PA wave equation is given by Eq. (1) [34],

$$\left(\nabla^2 - \frac{1}{v^2}\frac{\partial^2}{\partial t^2}\right) p(\boldsymbol{r}, t) = \frac{\beta}{\kappa v^2}\frac{\partial^2 T(\boldsymbol{r}, t)}{\partial t^2} \tag{1}$$

Where p($\boldsymbol{r}$, t) stands for the PA wave pressure in time t and position $\boldsymbol{r}$. β is the thermal volumetric expansion constant, κ is the isothermal compressibility, v is the speed of sound, and T($\boldsymbol{r}$,t) represents the temperature change in time t and position r. The left side of the equation expresses the acoustic wave emitted in the sample while the right side expresses the source of the acoustic wave [35]. The acoustic source also consists of two parts: the temporal and radial parts, respectively. The temporal part includes the laser parameters which are the heat source, the radial part contains the acoustic wave parameters.

In view of the many studies in the literature, the solutions are implemented on an imaginary spherical object (SO) heated by the laser as shown in Fig. 1. Furthermore, there is a relationship among the sensor position r, the radius R of the heated SO, the speed of sound v, and the wave propagation time t, as in Eq. (2).

$$\frac{r-R}{v} < t < \frac{r+R}{v} \tag{2}$$

There are many approaches in the literature for solving the PA wave equation [30–35]. We focus the solution of Erkol et al. given in Eq. (5) because they carried out the time domain solution of the PA wave equation by taking the Gaussian function in both parts of the source function. [36,37].

First of all, Erkol et al. [36,37] carried out the frequency domain solution of PA wave equation given in Eq. (3) ($r > R$) by taking the Gaussian function for the temporal part of the source func-

tion and the Heaviside function for the spatial part of the source function.

$$p(r,\omega) = ip_0\frac{v}{r}\frac{exp\left(-\frac{\tau_p^2\omega^2}{2}+i\frac{\omega}{v}r\right)}{\omega^2}\left[\frac{\omega}{v}Rcos\left(\frac{\omega}{v}R\right)-sin\left(\frac{\omega}{v}R\right)\right] \quad (3)$$

Where τ_p is the pulse duration of the laser, p_0 is the initial pressure.

Then, Erkol et al. obtained a partial PA wave frequency domain solution given in Eq. (4) by applying the Gaussian function for both parts of the source function to the frequency domain solution of the PA wave equation given by Eq. (3). In this way, they thought that they would reach a more realistic PA wave equation time domain solution. The main distinction between Eqs. (3) and (4) is that it is the frequency domain solutions of the PA wave equation obtained by using different source functions. Since their aim was to realize the time domain solution of the PA wave equation, they passed to the time domain solution without realizing the exact solution of Eq. (4):

$$p(r,\omega) = \frac{p_0}{2\pi}\frac{1}{vr}exp\left(-\frac{\tau_p^2\omega^2}{2}\right)\times\left\{\int_0^R r' exp\left(-\frac{r'^2}{2\tau^2}\right)\left[exp\left[i\frac{\omega}{v}\left(r-r'\right)\right]-exp\left[i\frac{\omega}{v}\left(r+r'\right)\right]\right]dr'\right\} \quad (4)$$

Where τ is the beamwidth of the laser. By applying the inverse Fourier transform to Eq. (4), they obtained the PA wave time domain exact solution given in Eq (5) [36,37],

$$p(r,t) = \frac{p_0\tau^2}{4r\sqrt{\left(\tau^2+\tau_p^2v^2\right)^3}}\exp\left[-\frac{2R(r-vt)+2(r-vt)^2+R^2}{2\tau_p^2v^2}-\frac{R^2}{2\tau^2}\right]$$

$$\left[\sqrt{2\pi}\tau(r-vt)\left\{erf\left[\frac{\tau^2(-r+R+vt)+R\tau_p^2v^2}{\sqrt{2}\tau\tau_pv\sqrt{\tau^2+\tau_p^2v^2}}\right]\exp\left[\frac{(r+R-vt)}{2\tau_p^2v^2}+\frac{\tau^2(r-vt)^2}{2\tau_p^2v^2\left(\tau^2+\tau_p^2v^2\right)}+\frac{R^2}{2\tau^2}\right]\right.\right.$$
$$\left.\left.+erf\left[\frac{\tau^2(r+R-vt)+R\tau_p^2v^2}{\sqrt{2}\tau\tau_pv\sqrt{\tau^2+\tau_p^2v^2}}\right]\exp\left\{\frac{\frac{\tau^2(-r+R+vt)+R\tau_p^2v^2}{\tau^2\left(\tau^2+\tau_p^2v^2\right)}+(r-vt)^2}{2\tau_p^2v^2}\right\}\right\}$$
$$\left.-2\tau v\sqrt{\tau^2+\tau_p^2v^2}\exp\left[\frac{(r-vt)^2}{2\tau_p^2v^2}\right]\left\{\exp\left[\frac{2R(r-vt)}{\tau_p^2v^2}\right]-1\right\}\right] \quad (5)$$

$$\theta\left(r-\left|R-vt\right|\right)\theta(-r+R+vt)$$

where θ is the Heaviside function. Since Erkol et al. did not solve the integral part of Eq. (4), the complete solution of this equation could not be obtained. In order to obtain the complete solution, we solved the integral part of Eq. (4) by applying several mathematical operations. The complex conjugate exponential functions in square brackets on the right side of Eq. (4) is extracted using the definition of the erfi (z) function (imaginary error function [45]). This makes it easier to extract the remaining part of the integral. In this case, the other part remaining in the integral has been extracted easier out of the integral by expanding to the Taylor series. This integration is presented earlier in our work [39]. The obtained solution of the integral is added to the other part of the equation, and Eq. (6), which is our improved theoretical model approach in this study is obtained at resulting of simplifications and mathematical arrangements. Because of these operations, the equation has been made more compact and suitable for the validation.

$$p(r,\omega) = \frac{p_0}{4\pi}\frac{\tau^2}{v^2r}exp\left(-\frac{\omega^2\tau_p^2}{2}-\frac{R^2}{\tau^2}-\frac{iR\omega}{v}+\frac{\omega\left(2irv-\omega\tau^2\right)}{2v^2}\right)$$
$$\left\{2vexp\left(\frac{R^2+\frac{\omega^2\tau^4}{v^2}}{2\tau^2}\right)\left(exp\left(\frac{2iR\omega}{v}\right)-1\right)\right.$$
$$\left.+\sqrt{2\pi}\tau\omega exp\left(\frac{R^2}{\tau^2}+\frac{iR\omega}{v}\right)\left(erfi\left(\frac{\omega\tau^2-iRv}{\sqrt{2}\tau v}\right)-erfi\left(\frac{\omega\tau^2+iRv}{\sqrt{2}\tau v}\right)\right)\right\} \quad (6)$$

For the validation of Eq. (6), experiments were carried out in the distilled water. For this purpose, Eq. (6) is arranged according to the constant parameters during the experiments and Eq. (7) is obtained. Values of constant parameters in the experiments are v = 1480 m/s, r = 2Rmm, R = 0.74 mm.

$$p(r,\omega) = \frac{p_0\tau^2}{4\pi(1480)^2\times1.48\times10^{-3}}$$
$$exp\left(-\frac{\omega^2\tau_p^2}{2}-\frac{(0.74\times10^{-3})^2}{\tau^2}+i5\times10^{-7}\omega-0.5\left(\frac{\omega\tau}{1480}\right)^2\right)$$
$$\left\{\begin{array}{l}2960exp\left(\frac{2.738\times10^{-7}}{\tau^2}+0.5\left(\frac{\omega\tau}{1480}\right)^2\right)\left(-1+exp\left(i1\times10^{-6}\omega\right)\right)+\\ \sqrt{2\pi}\tau\omega exp\left(\frac{5.476\times10^{-7}}{\tau^2}+i5\times10^{-7}\omega\right)\\ \left(erfi\left(\frac{-i0.74\times10^{-3}}{\tau\sqrt{2}}+\frac{\omega\tau}{1480\sqrt{2}}\right)-erfi\left(\frac{i0.74\times10^{-3}}{\tau\sqrt{2}}+\frac{\omega\tau}{1480\sqrt{2}}\right)\right)\end{array}\right\} \quad (7)$$

3. Experimental setup for validation

The experimental setup is depicted schematically in Fig. 2. Distilled water was chosen for the validation because it is frequently used in applications and a homogeneous medium that has physical parameters known. The theoric model to be validated involves strong absorption state. The strong absorption expresses states in which the radius of the laser beam (a) much larger than or comparable to the penetration depth ($1/\alpha$) [44,46]. The laser diode wavelength was determined 1550 nm because of the existence of the strong absorption peak of distilled water (approximate α >10 cm^{-1} [47]) at 1550 nm. A laser diode (LPSC-1550-FC Pigtailed Laser Diode, Max Power 100 mW, Thorlabs Inc.) operating at a wavelength of 1550 nm was used as the light source. The laser diode used in the pigtail, FPL1055 T Fabry-Perot Laser Diode with the Gaussian shaped has 300 mW output power when used as pulsed. The output power of the laser drops to 100 mW with losses during the

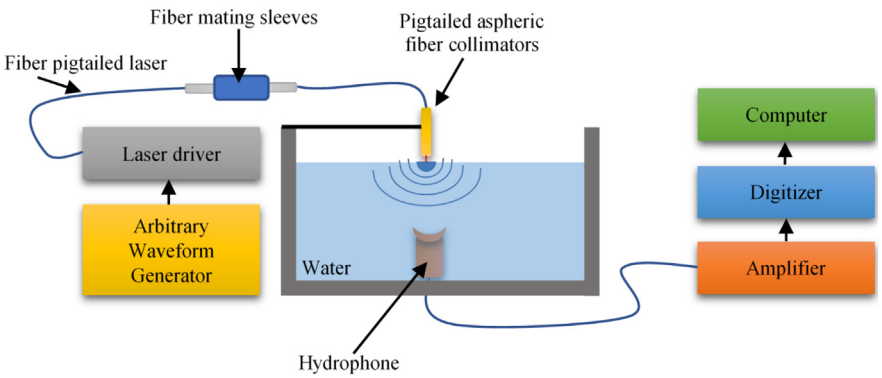

Fig. 2. Block diagram of the experimental setup for the validation.

laser beams are being coupled with optical fiber. When the laser coupled to the optic fiber (SMF-28-J9, core diameter 9 μm, Thorlabs Inc.), the correspondence of the laser beam width is regarded as the mode field diameter which is 10.4 μm in this work. The aspheric fiber collimators (CFS2-1550, CFS5-1550, Thorlabs Inc.) were used at the Pigtail Laser diode output. Since the input mode field diameter of the aspheric fiber collimator is the same as the output mode field diameter of the fiber, the collimator and fiber are compatible. According to the catalog information of the aspherical collimator (CFS2-1550), the effective focal length is 2.03 mm and the diameter of $1/e^2$ is 0.38 mm. In other words, the beam diameter of the laser which strikes from the height of 2.03 mm to the water surface the will be 0.7714 mm due to multiply the product of the two values given in the previous line. It is also the diameter of the spherical object. The diameter of the SO with the given calculation is compatible with the diameter the SO calculated by the PA method to be mentioned in the below section. A driver module (Picolas LDP-V 50–100 V3.3) was used to drive the laser diode. The pulsed signal generated by the arbitrary/function generator (AFG3021B, Tektronix) is applied to the trigger pulse input of this module. In this way, Pulse Width Modulation (PWM) signals with the high signal to noise ratio (SNR) were applied. The theoretical approach presented includes free boundary conditions. The experiment medium can be regarded as the free boundary condition due to the wavelength of the acoustic signal much bigger than the absorption coefficient of the medium [44]. The experiment was carried out in a cylindrical measuring cup of 20 cm in diameter and height. The presented theoric model also focuses on exploring the fineness of an exact solution to the PA equation for the spherical symmetric wave propagation. The time-domain bipolar waveforms of the experimentally derived PA signals are consistent with the free boundary, the spherical waveforms presented by Sigrist in his study [46]. Therefore, it is seen that the experimental setup is very suitable for Eq. (7) to be verified. As an acoustic transducer, A membrane hydrophone (HMA-0200, Onda Inc.) is placed at 2 mm below from the surface of a transparent container filled with distilled water. The HM Series membrane hydrophones are designed to measure ultrasonic signals. It has a flat frequency response and the bandwidth is in the range of 0.5 to 45 MHz. Nominal Sensitivity of the hydrophone is 100 nV/Pa. Because the amplitude of the detected signal from the detector is at μV levels, the signal is firstly amplified using a 40 dB preamplifier (Boteg Inc.). In this preamplifier design architecture, AD817 operational amplifiers (50 MHz Unity Gain Bandwidth, 350 V/ms Slew Rate, Analog Devices Inc.) are used. This ensures that the bandwidth of the generated PA signal and the preamplifier match each other. In addition, the high output current differential line driver AD815 (low harmonic distortion of –66 dB@1 MHz into 200 Ω, 120 MHz bandwidth, Analog Devices Inc.) used in the preamplifier has the ability to drive unlimited capacitive loads while maintaining excellent signal integrity. Then, for the obtaining the acoustic signal with the high SNR used the ultralow noise voltage-controlled amplifier AD8331-EVAL module as a final amplifier (Ultralow noise: Voltage noise 0.74 nV/√Hz, Current noise 2.5 pA/√Hz, 3 dB bandwidth 120 MHz, Analog Devices Inc.). When the HI (high gain) mode of this module is activated, the signal gain can be increased to 55.5 dB. After the amplification process, the received signals were measured with Picoscope (3206MSO, 200 MHz analog bandwidth, 1 GS/s real-time sampling, 512 MS buffer memory) as both an oscilloscope and also a data logger. Picoscope has also features a spectrum analyzer and the frequency domain measurement. The spectrum analyzer in this instrument is of the Fast Fourier Transform (FFT) type, which, unlike a conventional sweep spectrum analyzer, can display the spectrum of a single nonrepeatable waveform. The experimental data obtained from the pc oscilloscope is then processed by Matlab software and rendered graphical. The average values for the FFT spectrum were obtained by taking 32764 samples from the Hamming window at a sampling rate of 62.5 MSa/s.

In this study, four different experiments have been carried out to investigate the effect of the proposed theoretical model approach, as well as the effects of the laser parameters on the frequency response of the generated PA signal. In these experiments, the laser pulse width and the beam widths are changed. In Table 2, the laser parameters used in these experiments are given in detail. In all experiments except for Experiment 3, laser beam widths were taken as 0.7714 μm, whereas in Experiment 3 this value was taken as 0.8791 μm. And laser pulse widths were taken as 30 ns, 60 ns, 200 ns and, 200 ns according to the experimental order (#1, #2, #3, #4). In addition, the laser pulse repetition frequency (PRF) was 50 kHz in all experiments. The results of these experiments are discussed in the next section.

4. Results and discussions

Erkol et al. solved the time-domain of the PA wave equation by applying the Gaussian function to the temporal and the spatial parts of the source function [36,37]. For this reason, we think that it is a more realistic solution than similar solutions in the literature. All experimental measurements were made in the distilled water to verify the theoretical model approach. The theoretical equations used for comparison in experimental verification are respectively Eq. (5) for time domain and Eq. (7) for frequency domain. In Fig. 3 the theoretical results obtained from Eq. (5) and the graphs of the measured values are plotted overlaid. The PA wave parameter values for the time domain theoretical calculation are given in Table 1. The PRF is applied at 50 kHz. In the measured time-domain values, when the laser pulse duration values increased, indicating that the amplitude of the obtained PA signal dropped. Since the PA wave

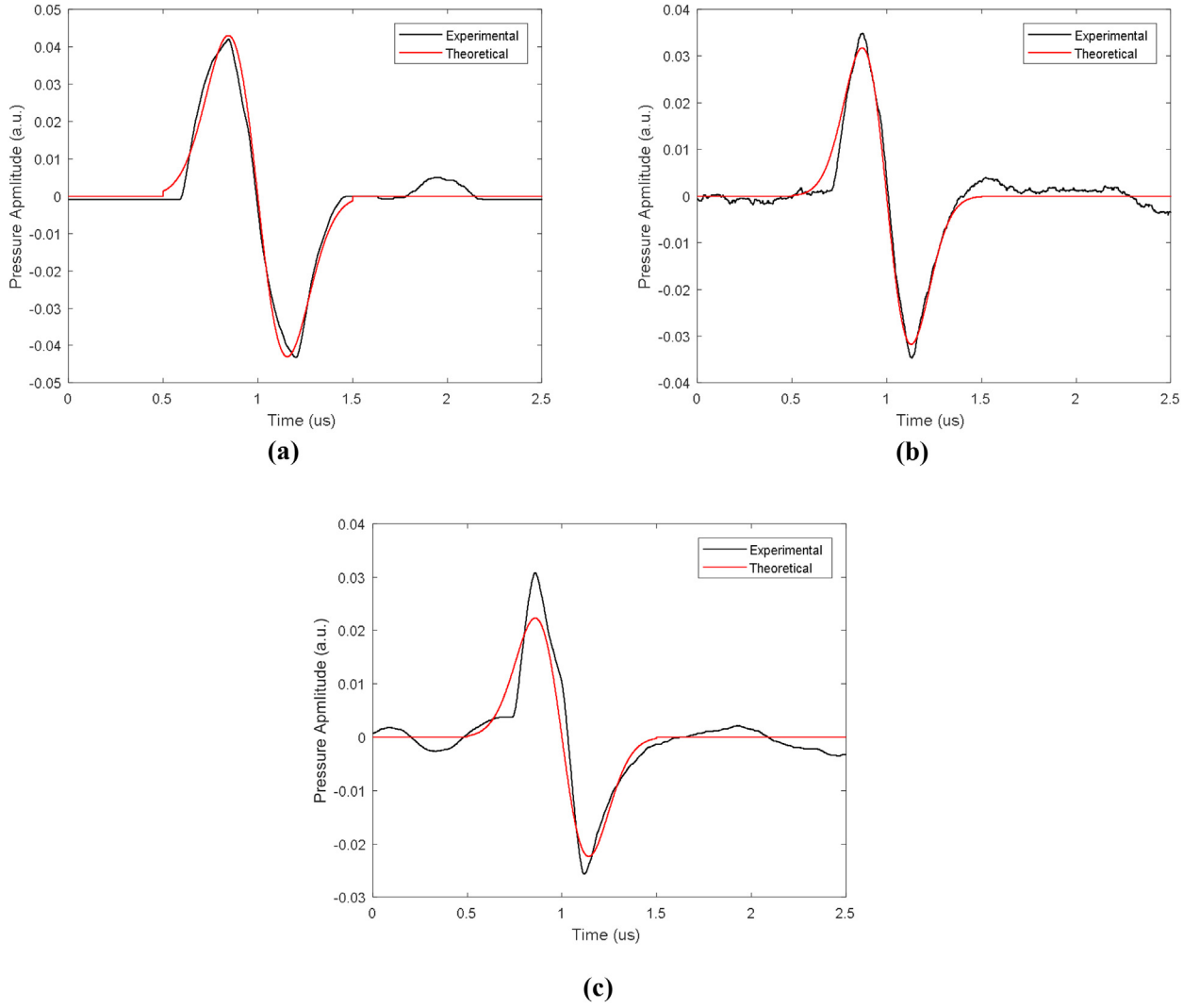

Fig. 3. The time response of the PA signal. (a) The pulse duration with 20 ns. (b) The pulse duration with 30 ns. (c) The pulse duration with 60 ns.

Table 1
The PA wave parameter values for the time domain.

Figure No	τ (mm)	τ_p (ns)
3.(a)	0.7714	20
3.(b)	0.7714	30
3.(c)	0.7714	60

Table 2
The PA wave parameter values for the frequency domain.

Figure No	τ (μm)	τ_p (ns)
5, Experiment #1	0.7714	30
5, Experiment #2	0.7714	60
6.(a)	0.7714	20
6.(b)	0.7714	30
6.(c)	0.7714	60
7, Experiment #3	0.8791	200
7, Experiment #4	0.7714	200

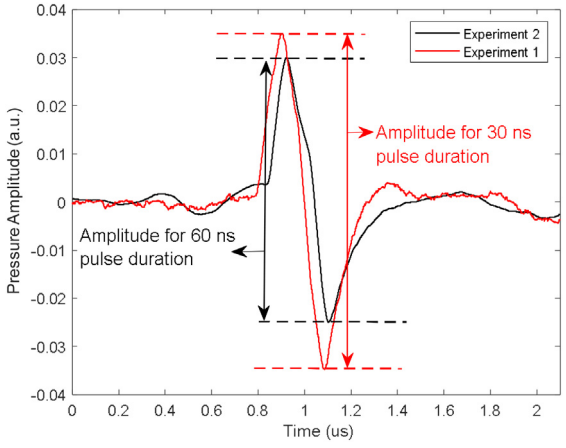

Fig. 4. The time response of the PA signal for the different pulse duration values with 0.7714 beam width.

time domain analysis does not constitute the main work of this study, we focused on the frequency domain solutions. However, extensive analysis of this issue has been reported in our previous work [39]. We used the time domain measurements in the calculation of the SO diameter, which will be mentioned in the following discussions.

For the spectral analysis, the diameter of the SO has been investigated primarily for use in the theoretical calculations. The SO diameter is one of the critical parameters that determine the frequency content of the produced PA signal. It is very difficult to accurately measure the diameter of objects buried in a liquid

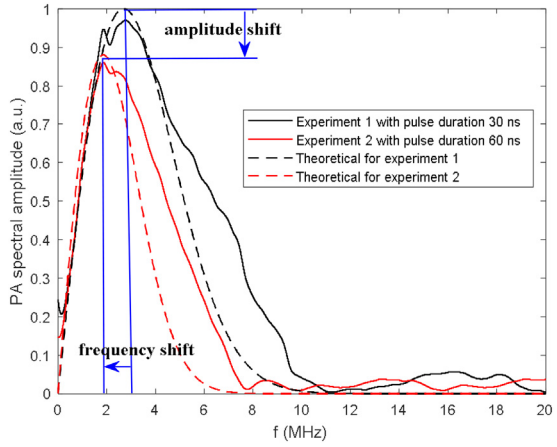

Fig. 5. The frequency domain of the two signals in Fig. 4: The theoretical and the experimental measurement results.

medium with micron accuracy using an optical microscope. For this reason, the object diameter is calculated by using ultrasonic and the PA methods [40]. In this study, we determined the diameter of the SO by making measurements from the time-domain image of the PA wave. When the medium is heated by an optical source, a SO absorbs optical energy, and then a forward-moving pressure wave occurs due to the thermoelastic process that takes place. Positive and negative pressure peaks form a standard N-shaped PA wave in the time domain. The time difference between these peak values is used to measure the diameter of the SO [41]. By measuring the time difference between these peak values, it is substituted in Eq. (8) and the diameter of the SO is calculated.

$$d = v(t_n - t_p) \tag{8}$$

Where t_p is the positive pressure peak time and t_n is the negative pressure peak time. In Fig. 3.(a), the $t_n - t_p$ value is measured approximately 0.5 μs. When this value is multiplied by the sound speed of the distilled water, we can calculate the diameter of the SO as 0.74 mm. The parameters used in the frequency domain measurements in the figures are given in Table 2 and the PRF is applied at 50 kHz.

In Fig. 4, the measured values of Fig. 3(b) and (c) are superimposed on each other in the time domain.

Fig. 5 shows both the theoretical and the experimental measurement results in the frequency domain of the two signals in Fig. 4 for the different pulse duration values with 0.7714 mm beam width. The difference in these two measurements is the pulse duration values. The Pulse duration is 30 ns for measurements with high amplitude and 60 ns for low amplitude measurements. Fig. 5 shows that our theoretical approach model and the experimen-

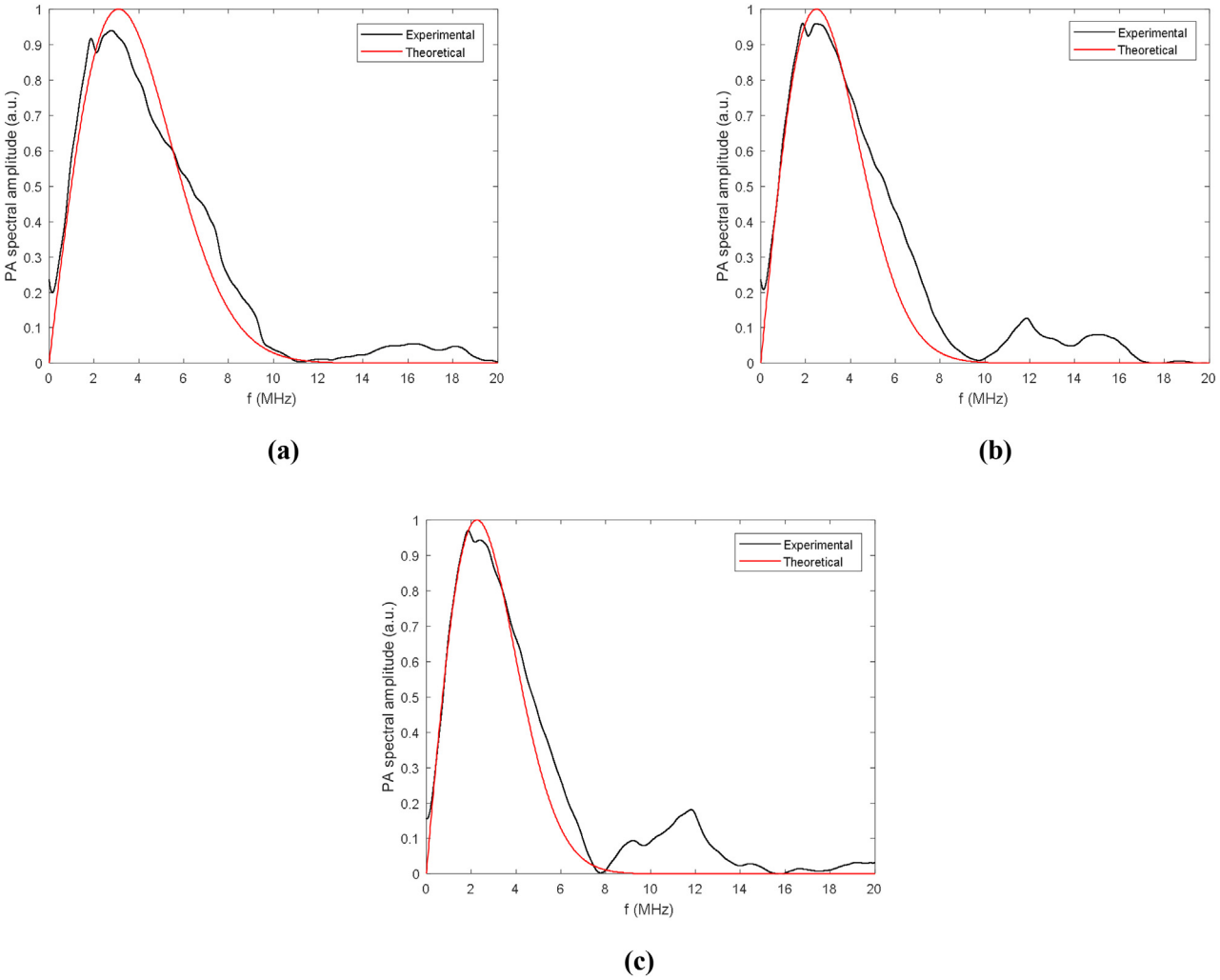

Fig. 6. The frequency domain of the PA signal: Theoretical and the experimental results of the measurements made according to the pulse duration with the different laser parameters in Table 2. (a) The pulse duration with 20 ns. (b) The pulse duration with 30 ns. (c) The pulse duration with 60 ns.

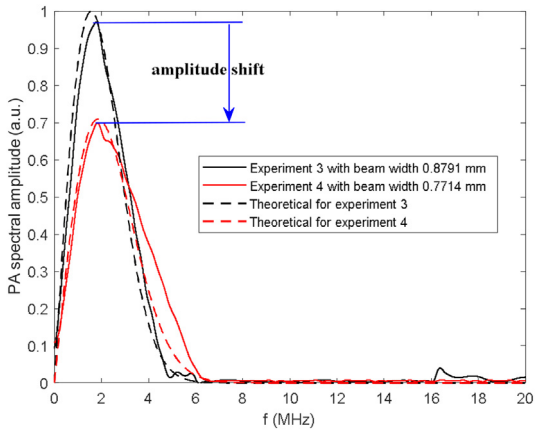

Fig. 7. The frequency domain of the PA signal: Theoretical and the experimental measurement results of two signals with the different beam widths.

tal measurement values are very consistent. For example, while the theoretical fundamental peak frequency of Experiment 1 was 2.783 MHz, this value was measured to be 2.683 MHz. With the theoretical approach, the fundamental peak value was found with an accuracy of ∓ 3.592%. Furthermore, the effect of the pulse duration on the spectral content and the spectral amplitude is clearly seen in Fig. 5. When the laser pulse energy is constant, high amplitude PA signals occur at small pulse durations [42]. For this reason, the shorter pulse durations together with a distortion in-depth resolution result in the larger wave amplitudes [37]. Also, the PA wave spectral content changes by the changing the pulse duration value and as the pulse duration increases, the resonance frequency shifts towards lower values. These are illustrated in Fig. 5. The disappearance of the high frequency content of the PA is undesirable in imaging applications, because the sample size to be displayed is directly proportional to the acoustic wave frequency [43].

Fig. 6 shows the theoretical and the experimental results of the measurements with the pulse duration with the different laser parameters. Compatibility of graphics clearly shows that the experimental results validate our theoretical model approach. Also, in the graphs, the fundamental frequency has shifted to lower values as the pulse duration increases.

Another laser parameter, which has a big effect on the PA signal, is the laser beam width. In Fig. 7, both the theoretical and the experimental measurement results of two signals are drawn with the different beam widths. Excitation of the medium by a laser pulse with the higher beam width causes a large part of the energy to be absorbed by absorbers in the medium. The result of this, the amplitude of the PA signal increases. As the beam width decreases, the temporal profile of the PA signal sharpens and transform into an n-shaped wave. In this case, the Gaussian spatial profile behaves like a Dirac delta and on the resulting signal and the effect of the laser parameters is destroyed. There are also differences in the spectral content of the PA signal. In contrast to the pulse duration, as the beam width increases, the resonance frequency of the signal approaches lower values. As can be seen in the graphs obtained in Fig. 7, our theoretical model approach has been confirmed to be very consistent with the measurements. While the theoretical fundamental peak frequency of Experiment 4 was 1.842 MHz, this value was measured to be 1.823 MHz. With the theoretical approach, the fundamental peak value was found with an accuracy of ± 1.042%. Table 3 shows the fundamental frequency values of the theoretical and experimental PA signals. According to the theoretical model approach, the fundamental frequency values obtained from the experimental measurement results were determined with an average accuracy of ∓ 4.212%.

Table 3
The fundamental frequency values of the PA signal, theoretical and experimental.

Figure No	*Theoretical* (MHz)	*Experimental* (MHz)	*Variation* (±%)
Experiment 1	2.683	2.783	3.592
Experiment 2	1.862	1.867	0.267
Experiment 3	1.562	1.774	11.950
Experiment 4	1.842	1.823	1.042

5. Conclusions

The theoretical model approach based on the development of the frequency domain solution of the PA wave equation for use in the PA pressure sensor designs to determine the fundamental frequency of the PA wave is presented. To verify the theoretical model approach, the PA test setup is established, and measurements are made in distilled water. The theoretical model approach shows that the PA frequency spectra obtained by experimentally and theoretically are compatible with each other. With these experimental measurements, we reported the correctness of our theoretical model approach. In the pulsed laser PA detection and spectroscopy applications, the fundamental frequency and the acoustic sensor resonance frequency of the PA signal produced must be as close as possible to each other so that the sensor frequency selectivity is increased and analyzes from the obtained signals can be performed effectively. With the theoretical model approach, the fundamental frequency values obtained from the experimental measurement results are determined with an average accuracy of ±4.212%. It is measured that this value decreased to ±0.267%. With the help of the theoretical model approach, we propose that more narrowband PA pressure sensors can be designed, and hence more precise detection can be possible. Furthermore, in this study, the effects of different laser parameters (pulse duration, laser beam width) on the spectral content of the obtained PA signal are analyzed.

Acknowledgments

This work was supported by the Research Fund of the Erciyes University. Project numbers FDK-2016-6811 and FDK-2016-6815. The authors would like to thank Erciyes University Clinical Engineering Research and Application Center for their support in the research activities among the staffs.

References

[1] T.G. Jones, M.K. Hornstein, A.C. Ting, Z.W. Wilkes, D.A. Lindwall, Underwater acoustic generation with narrow and broadband lasers, J. Acoust. Soc. Am. 123 (5) (2008) 3953.
[2] S. Sethuraman, J.H. Amirian, S.H. Litovsky, R.W. Smalling, S.Y. Emelianov, Spectroscopic intravascular photoacoustic imaging to differentiate atherosclerotic plaques, Opt. Express 16 (5) (2008) 3362–3367.
[3] E.B. Samson, B.S. Goldschmidt, P.J. Whiteside, A.S. Sudduth, J.R. Custer, B. Beerntsen, J.A. Viator, Photoacoustic spectroscopy of β-hematin, J. Opt. 14 (6) (2012), 065302.
[4] A. Gijsbertsen, D. Bicanic, J.L.W. Gielen, M. Chirtoc, Rapid, non-destructive and non-contact inspection of solid foods by means of photothermal radiometry; thermal effusivity and initial heating coefficient, Infrared Phys. Technol. 45 (2) (2004) 93–101.
[5] G.A. Askar'yan, A.M. Prokhorov, G.F. Chanturiya, G.P. Shipulo, The effects of a laser beam in a liquid, Sov. Phys. JETP 17 (6) (1963) 1463–1465.
[6] W.B. Jackson, N.M. Amer, A.C. Boccara, D. Fournier, Photothermal deflection spectroscopy and detection, Appl. Opt. 20 (8) (1981) 1333–1344.
[7] A. Rosencwaig, Photoacoustic spectroscopy of biological materials, Science 181 (4100) (1973) 657–658.
[8] S. Oda, T. Sawada, H. Kamada, Determination of ultra-trace cadmium by laser-induced photoacoustic absorption spectrometry, Anal. Chem. 50 (7) (1978) 865–867, http://dx.doi.org/10.1021/acs.analchem.6b03286.
[9] A.C. Tam, Applications of photoacoustic sensing techniques, Rev. Mod. Phys. 58 (2) (1986) 381, http://dx.doi.org/10.1103/RevModPhys.58.381.
[10] F. El-Akkad, A.R. Farhan, Photoacoustic determination of the absorption spectra in $Hg_{1-x}Zn_xTe$ alloys, J. Phys. D Appl. Phys. 28 (9) (1995) 1958.

[11] H.A. MacKenzie, G.B. Christison, P. Hodgson, D. Blanc, A laser photoacoustic sensor for analyte detection in aqueous systems, Sens. Actuators B Chem. 11 (1-3) (1993) 213–220, http://dx.doi.org/10.1016/0925-4005(93)85257-B.
[12] H.A. MacKenzie, H.S. Ashton, Y.C. Shen, J. Lindberg, P. Rae, K.M. Quan, S. Spiers, Blood glucose measurements by photoacoustics, in: Biomedical Optical Spectroscopy and Diagnostics (p. BTuC1), Optical Society of America, 1998, http://dx.doi.org/10.1364/BOSD.1998.BTuC1.
[13] G.B. Christison, H.A. MacKenzie, Laser photoacoustic determination of physiological glucose concentrations in human whole blood, Med. Biol. Eng. Comput. 31 (3) (1993) 284–290, http://dx.doi.org/10.1007/BF02458048.
[14] H.A. MacKenzie, H.S. Ashton, S. Spiers, Y. Shen, S.E. Freeborn, J. Hannigan, J. Lindberg, P. Rae, Advances in photoacoustic noninvasive glucose testing, Clin. Chem. 45 (9) (1999) 1587–1595.
[15] J.G. Camilotti, A. Somer, G.F. Costa, M.A. Ribeiro, C. Bonardi, G.K. Cruz, et al., The phase-resolved photoacoustic method to indicate chemical assignments of paracetamol, Spectrochim. Acta A. Mol. Biomol. Spectrosc. 121 (2014) 719–723.
[16] F.J. Harren, J. Mandon, S.M. Cristescu, Photoacoustic spectroscopy in trace gas monitoring, in: Encyclopedia of Analytical Chemistry, 2000, ISBN: 10.1002/9780470027318.a0718.pub2.
[17] A. Elia, P.M. Lugarà, C. Di Franco, V. Spagnolo, Photoacoustic techniques for trace gas sensing based on semiconductor laser sources, Sensors 9 (12) (2009) 9616–9628, http://dx.doi.org/10.3390/s91209616.
[18] A. Miklós, P. Hess, Z. Bozóki, Application of acoustic resonators in photoacoustic trace gas analysis and metrology, Rev. Sci. Instrum. 72 (4) (2001) 1937–1955, http://dx.doi.org/10.1063/1.1353198.
[19] V. Zeninari, B. Parvitte, D. Courtois, V.A. Kapitanov, Y.N. Ponomarev, Methane detection on the sub-ppm level with a near-infrared diode laser photoacoustic sensor, Infrared Phys. Technol. 44 (4) (2003) 253–261.
[20] J.W. Choi, M.J. You, S.W. Choi, S.Y. Woo, Photoacoustic laser doppler velocimetry using the self-mixing effect of RF-excited CO_2 laser, J. Opt. Soc. Korea 8 (4) (2004) 188–191, http://dx.doi.org/10.3807/JOSK.2004.8.4.188.
[21] A.A. Kosterev, F.K. Tittel, Ammonia detection by use of quartz-enhanced photoacoustic spectroscopy with a near-IR telecommunication diode laser, Appl. Opt. 43 (33) (2004) 6213–6217.
[22] T. Rück, R. Bierl, F.M. Matysik, Low-cost photoacoustic NO_2 trace gas monitoring at the pptV-level, Sens. Actuators A Phys. 263 (2017) 501–509.
[23] A. Elia, P.M. Lugarà, C. Giancaspro, Photoacoustic detection of nitric oxide by use of a quantum-cascade laser, Opt. Lett. 30 (9) (2005) 988–990.
[24] D. Kumar, S. Gautam, S. Kumar, S. Gupta, H.B. Srivastava, S.N. Thakur, R.C. Sharma, Ultrasensitive photoacoustic sensor based on quantum cascade laser spectroscopy, Spectrochimica Acta Part A 176 (2017) 47–51.
[25] K. Chen, Z. Gong, Q. Yu, Fiber-amplifier-enhanced resonant photoacoustic sensor for sub-ppb level acetylene detection, Sens. Actuators A Phys. 274 (2018) 184–188.
[26] P. Mohajerani, S. Kellnberger, V. Ntziachristos, Frequency domain optoacoustic tomography using amplitude and phase, Photoacoustics 2 (3) (2014) 111–118, http://dx.doi.org/10.1016/j.pacs.2014.06.002.
[27] R.E. Kumon, C.X. Deng, X. Wang, Frequency-domain analysis of photoacoustic imaging data from prostate adenocarcinoma tumors in a murine model, Ultrasound Med. Biol. 37 (5) (2011) 834–839, http://dx.doi.org/10.1016/j.ultrasmedbio.2011.01.012.
[28] D. Wu, L. Huang, M.S. Jiang, H. Jiang, Contrast agents for photoacoustic and thermoacoustic imaging: a review, Int. J. Mol. Sci. 15 (12) (2014) 23616–23639, http://dx.doi.org/10.3390/ijms151223616.
[29] S.Y. Nam, S.Y. Emelianov, Array-based real-time ultrasound and photoacoustic ocular imaging, J. Opt. Soc. Korea 18 (2) (2014) 151–155, http://dx.doi.org/10.3807/JOSK.2014.18.2.151.
[30] M.W. Sigrist, F.K. Kneubühl, Laser-generated stress waves in liquids, J. Acoust. Soc. Am. 64 (6) (1978) 1652–1663, http://dx.doi.org/10.1121/1.382132.
[31] H.M. Lai, K. Young, Theory of the pulsed optoacoustic technique, J. Acoust. Soc. Am. 72 (6) (1982) 2000–2007, http://dx.doi.org/10.1121/1.388631.
[32] C.G.A. Hoelen, F.F.M. De Mul, R. Pongers, A. Dekker, Three-dimensional photoacoustic imaging of blood vessels in tissue, Opt. Lett. 23 (8) (1998) 648–650, http://dx.doi.org/10.1364/OL.23.000648.
[33] I.G. Calasso, W. Craig, G.J. Diebold, Photoacoustic point source, Phys. Rev. Lett. 86 (16) (2001) 3550, http://dx.doi.org/10.1103/PhysRevLett.86.3550.
[34] L.V. Wang, H.I. Wu, Biomedical Optics: Principles and Imaging, John Wiley & Sons, 2012, ISBN: 9780470177006.
[35] L.V. Wang, Tutorial on photoacoustic microscopy and computed tomography, Ieee J. Sel. Top. Quantum Electron. 14 (1) (2008) 171–179, http://dx.doi.org/10.1109/JSTQE.2007.913398.
[36] H. Erkol, E. Aytac-Kipergil, M.U. Arabul, M.B. Unlu, Analysis of laser parameters in the solution of photoacoustic wave equation, March Photons Plus Ultrasound: Imaging and Sensing 2013, Vol. 8581, International Society for Optics and Photonics, 2013, pp. 858136, http://dx.doi.org/10.1117/12.2003844.
[37] H. Erkol, E. Aytac-Kipergil, M.B. Unlu, Photoacoustic radiation force on a microbubble, Phys. Rev. E 90 (2) (2014), 023001, http://dx.doi.org/10.1103/PhysRevE.90.023001.
[38] Z. Zhao, S. Nissila, O. Ahola, R. Myllyla, Production and detection theory of pulsed photoacoustic wave with maximum amplitude and minimum distortion in absorbing liquid, IEEE Trans. Instrum. Meas. 47 (2) (1998) 578–583, http://dx.doi.org/10.1109/19.744208.
[39] T.E. Tabaru, Ş.E. Hayber, Ö.G. Saraçoğlu, Frequency domain analysis of laser and acoustic pressure parameters in photoacoustic wave equation for acoustic pressure sensor designs, Curr. Opt. Photon. 2 (3) (2018) 250–260, http://dx.doi.org/10.3807/COPP.2018.2.3.250.
[40] E. Strohm, I. Gorelikov, N. Matsuura, M. Kolios, Photoacoustic spectral characterization of perfluorocarbon droplets, February Photons Plus Ultrasound: Imaging and Sensing 2012, Vol. 8223, International Society for Optics and Photonics, 2012, pp. 82232F.
[41] G.J. Diebold, M.I. Khan, S.M. Park, Photoacoustic ïsignaturesöf particulate matter: optical production of acoustic monopole radiation, Science 250 (4977) (1990) 101–104.
[42] E.A. Kipergil, H. Erkol, S. Kaya, G. Gulsen, M.B. Unlu, An analysis of beam parameters on proton-acoustic waves through an analytic approach, Phys. Med. Biol. 62 (12) (2017) 4694.
[43] A.G. Gertsch, N.L. Bush, D.C.C. Birtill, J.C. Bamber, Toward characterizing the size of microscopic optical absorbers using optoacoustic emission spectroscopy Photons Plus Ultrasound: Imaging and Sensing 2010, Vol. 7564, International Society for Optics and Photonics, 2010, pp. 75641M.
[44] V.E. Gusev, A.A. Karabutov, Laser optoacoustics, in: NASA STI/Recon Technical Report A, 1991, pp. 93.
[45] M. Mori, A method for evaluation of the error function of real and complex variable with high relative accuracy, Publ. Res. Inst. Math. Sci. 19 (3) (1983) 1081–1094.
[46] M.W. Sigrist, Laser generation of acoustic waves in liquids and gases, J. Appl. Phys. 60 (7) (1986) R83–R122.
[47] G.M. Hale, M.R. Querry, Optical constants of water in the 200-nm to 200-μm wavelength region, Appl. Opt. 12 (3) (1973) 555–563.

Biographies

Timuçin Emre Tabaru received the M.S. and Ph.D. degrees in the Department of Electrical-Electronics Engineering from Erciyes University, Kayseri, Turkey, in 2014 and 2018, respectively. He is working as a lecturer at The Clinical Engineering Research and Application Center, Erciyes University. His current research interests are fiber optic sensors, optical signal processing, photoacoustic detection, photonic sensors, biomedical optics and electro-optical instruments. He has been involved in many research and development projects as a project manager and researcher.

Sekip Esat Hayber received the M.S. and Ph.D. degrees in the Department of Electrical-Electronics Engineering from Erciyes University, Kayseri, Turkey, in 2011 and 2018, respectively.He is working as a lecturer at the Department of Electronic and Automation, Kırşehir Ahi Evran University, Turkey. His research involves optic and fiber optic detection, optical fiber sensing system, photonic sensors.